Proceedings 10th NUMGE 2023
10th European Conference on Numerical Methods in Geotechnical Engineering
Zdravkovic L, Kontoe S, Taborda DMG, Tsiampousi A (eds)

https://doi.org/10.53243/NUMGE2023-168

One-point integrated hourglass-enhanced u-U elements with mortar fluid-phase contact and Sanisand interface

J. Machaček[1], P. Staubach[2]

[1] *Institute of Geotechnics, Technische Universität Darmstadt, Darmstadt, Germany*
[2] *Chair of Geotechnics, Bauhaus-Universität Weimar, Germany*

ABSTRACT: Realistic simulation of coupled geotechnical boundary value problems using the finite element method places high demands on element formulations, constitutive soil models and interface modelling. This applies to their (mathematical) formulation as well as their (robust) implementation. A novel two-phase Mortar contact is presented which allows to accurately model interface behaviour for element formulations discretising both the solid- and the water-displacement (u-U formulation). For the latter, a one-point integration is presented, which prevents locking for nearly constant volume conditions. The robustness and capability of the implementations are demonstrated by the back-calculation of a shaking-table centrifuge test. The Sanisand-04 constitutive model is used herein to describe both the soil and the soil-structure interface behaviour. The results of the u-U elements are compared to results obtained with (classical) u-p elements.

Keywords: coupled dynamics; element formulations; interface; hourglass stiffness; mortar contact

1 INTRODUCTION

In most finite element codes used in geotechnics, only the u-p element formulation is implemented for the simulation of coupled (dynamic) analyses. However, alternative formulations, such as the u-U or u-p-U formulation may offer advantages for some boundary values problems (BVPs). The advantages and disadvantages of these formulations with respect to locking effects, computational performance, application to analyses involving contact and dynamic problems with high frequencies are discussed in this work. The development of reduced integrated hydro-mechanically coupled finite elements enhanced by hourglass stiffness for the fluid phases is presented in this paper. Moreover, since u-U elements discretise the fluid displacement, a Mortar contact disretisation scheme for the fluid phase is proposed. The advantages of elements with pore fluid displacement degree of freedom in contact analyses is outlined based on the practical example of earthquake stability of a strip footing. For this purpose, shaking table centrifuge tests performed by (Zeybek and Madabhushi, 2017) are back-calculated and the simulation results are compared to the measurements. A special feature of these centrifuge tests is the high loading frequency of 50 Hz (in model scale), which brings to the fore the question of the applicability of so-called u-p elements, which is often of high relevance in geotechnical engineering (Staubach & Machaček, 2019). All numerical schemes developed are implemented in the finite element programme numgeo (Machaček et al., 2021 and Staubach et al., 2022a, www.numgeo.de), which is freely available.

2 FINITE ELEMENT FORMULATIONS

numgeo offers a variety of element formulations based on the theory of porous media, which allow a realistic simulation of saturated and unsaturated soils - also in dynamic calculations (with simultaneous consolidation). In addition to the well-known u-p formulation, the so-called u-p-U and u-U formulations are also offered, which discretise not only the solid displacement (u) or the pore water pressure (p) but also the displacement of the pore fluids (U) and are particularly suitable for calculations involving high-frequencies. The u-U and u-p-U elements have been implemented and validated in numgeo (Staubach & Machaček, 2019). The u-p element formulation neglects the relative acceleration between solid and water (the accelerations are assumed identical). In order to satisfy the Lashenskaya-Babuška-Brezzi condition (Boffi et al. 2013) and at the same time ensure good convergence in contact simulations (Staubach et al. 2022c), 27-node brick elements with quadratic interpolation of displacements and linear interpolation of pore water pressure were used in case of the u-p formulation. In case of the u-U formulation, reduced integrated, hourglass enhanced 8-node brick elements with linear interpolation of the solid and water displacements were chosen. The different element formulations used in the present study are given in Figure 1.

To eliminate the volumetric locking caused by the inability of linear shape functions to properly approximate the incompressibility condition at full integration, elements with reduced integration of the

solid and fluid displacement are implemented in numgeo.

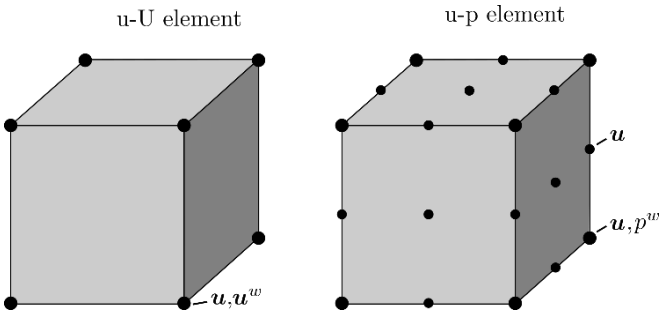

Figure 1. Element formulations used for the simulation of the shaking table tests in Section 5. p^w is the pore fluid pressure, u and u^w denote the displacements of the solid phase and the pore fluid phase, respectively.

Since reduced integration is associated with rank deficiencies, stabilization of these elements is required. For this purpose, the method according to (Flanagan & Belytschko, 1981) was implemented in numgeo, where the element stiffness is stabilized by the addition of an artificial stiffness $\boldsymbol{K}^{s/f,HG}$:

$$\begin{aligned}\boldsymbol{K}^{s/f,e} &= \boldsymbol{K}^{s/f,1Pt} + \boldsymbol{K}^{s/f,HG} \\ &= \boldsymbol{K}^{s/f,1Pt} + \kappa^{s/f,HG}\mathrm{d}\Omega^e \sum^{\alpha} \gamma_\alpha \gamma_\alpha,\end{aligned} \tag{1}$$

where $\boldsymbol{K}^{s/f,1Pt}$ is the conventional element stiffness matrix evaluated at one integration point (located in the centre of the element) for the solid phase (s) or fluid phase (f), respectively. γ_α are the hourglass shape vectors according to (Flanagan & Belytschko, 1981). $\kappa^{s/f,HG} > 0$ controls the stiffness of the hourglass resistance and can be chosen arbitrarily and, in its simplest form, is assumed constant throughout the simulation. For the present study $\kappa^{s/f,HG}$ are calculated as follows:

$$\kappa^{s/f,HG} = c^{s/f,HG}\frac{\partial \boldsymbol{N}}{\partial \boldsymbol{x}}\frac{\partial \boldsymbol{N}}{\partial \boldsymbol{x}}. \tag{2}$$

Therein, $c^{s/f,HG}$ have the physical meaning of stiffness. For the solid phase, $c^{s,HG}$ is typically in the range of $0.01G^s$, with G^s being the shear modulus of the solid. For the water phase, we propose to link $c^{f,HG}$ to the bulk modulus of the fluid phase K^f. $c^{f,HG} \approx 0.01K^f - 0.05K^f$ has provided good stabilisation of the elements in previous investigations without significantly influencing the simulation results. If the bulk modulus of pure water is used in the simulations, it is recommended to choose a lower value for $c^{f,HG}$.

3 CONTACT MECHANICS

3.1 Contact discretisation

To date, there has been little research on the treatment of contact constraints for element formulations discretising fluid displacements. To enforce contact constraints, contact forces are required which keep surfaces from intersection or, in some cases, from separating from each other. The contact discretisation is used to calculate the distance and relative motion of a surface pairing and eventually integrates the contact stresses to obtain contact forces. The shortest distance between two surfaces using an iso-parametric description in 2D can be calculated by:

$$\left[\sum_J^{nnode} N_J^{(2)}\left(\overline{\xi^{(2)}}\right)\boldsymbol{x}_J^{(2)} - \boldsymbol{x}_I^{(1)}\right] \cdot \boldsymbol{x}_{,\xi}^{(2)}\left(\overline{\xi^{(2)}}\right) = 0. \tag{3}$$

An orthogonal projection of the coordinates $\boldsymbol{x}_I^{(1)}$ of slave node *I* onto the master surface $\Gamma_c^{(2)}$ is performed for this purpose. $\boldsymbol{x}_J^{(2)}$ are the coordinates of node *J* of the master surface and *nnodes* are the total number of nodes of the face of the element belonging to the master surface. This is done by enforcing the tangential vector of the master surface $\boldsymbol{x}_{,\xi}^{(2)}\left(\overline{\xi^{(2)}}\right)$ to be orthogonal to the normal gap vector with minimum magnitude between the master surface and slave node *I*. The projection for the 3D case is schematically shown in Figure 2. This projection is performed for both surfaces of the surface pair and typically for a larger number of points than existing nodes of surfaces. This is advantageous since the strongly non-linear distribution of contact distances is better approximated. Such schemes are often denoted as Mortar contact methods, of which two different classes (element-based and segment-based) are implemented in numgeo (see Staubach et al., 2022a).

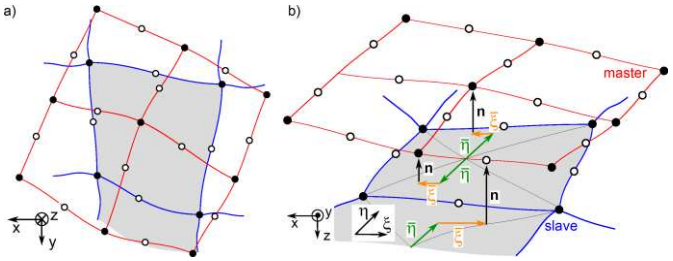

Figure 2. Evaluation of the convective coordinates of the slave surface for 3D analyses. Figure a) shows the top-view on the surfaces. The exemplary evaluation of the convective coordinates of the slave surface by projection to three master nodes is given in Figure b)

For element formulations discretising the fluid displacement, special considerations must be made. While the u-p elements do not discretise the movement of the pore fluid explicitly, the u-U element formulation does. Therefore, the contact constraints have to be enforced for the pore fluid movement as well, i.e. the

pore fluid has to be prevented to move into the paired object. For some BVPs, this can also be realised by coupling the solid movement to the fluid movement along the contact surface using multi-point constraints. However, a separation of the phases along the interface is then impossible. In addition, for most BVPs it is not possible to constrain the displacement only in normal direction of the contact, i.e. in case of a pile with constantly changing normal vector in circumferential direction.

In order to correctly model the interface using the u-U formulation, the contact discretisation and contact enforcement are performed separately for the solid and the fluid phases. Thus, contact forces are distinguishable and the constitutive contact behaviour can be treated separately. The total normal contact stress t_N is the sum of the effective normal contact stress t'_N and the normal fluid contact stress t^f_N, viz.

$$t_N = t'_N + t^f_N. \tag{4}$$

To determine t^f_N, the same contact discretisation and contact enforcement techniques as for the solid phase are used. The residuum of contact forces is extended contribution of the fluid phase, yielding

$$r^C_I = \int_{\Gamma^{C,s}} \boldsymbol{t}^{C,s}_I d\,\Gamma^{C,s} + \int_{\Gamma^{C,f}} \boldsymbol{t}^{C,f}_I\, d\Gamma^{C,f}, \tag{5}$$

where $\boldsymbol{t}^{C,s}_I$ is the contact stress of the solid phase and $\boldsymbol{t}^{C,f}_I$ the contact stress of the fluid phase. $\Gamma^{C,s}$and $\Gamma^{C,f}$ are the active contact areas of the solid and the fluid phase, respectively.

Essentially, the Mortar algorithms are applied to the fluid phase as well. Conceptually, this can be viewed as if there were two meshes with identical numbers of nodes but different positions. The contact operations are performed for both meshes independently and the contact forces are distributed to the two phases according to the relative distance of each phase to the paired object.

3.2 Constitutive Contact Model

A simple Coulomb friction cannot capture the strongly non-linear and history-dependent interface behaviour of granular media. One solution to this is to introduce discrete interface elements, which constitutive description is the same as for the continuum. However, such interface elements are limited to merely small relative tangential movement of the contact pair. To overcome this problem, a zero-thickness formulation in the framework of the Mortar contact discretisation scheme is presented in this section, which allows to directly adopt existing continuum models as interface models. For this, the state variables such as stress, density and any additional internal variables must be known in the interface. Using existing approaches (Stutz et al., 2016), mostly formulated for hypoplastic models, the stress state in the interface element is not necessarily identical to the stress state of the adjacent continuum. However, initial jump (prior to shearing) in any stress component between interface and continuum violates the static stress equilibrium if homogeneity is assumed.

To resolve the aforementioned problems, a novel approach is presented here, where the components of normal stress in the interface are the same as those of the adjacent continuum. The normal components of the stress tensor of the interface $\boldsymbol{T}^{\text{interface}}$ are obtained from the adjacent continuum element using

$$\boldsymbol{T}^{\text{interface}} = \sum_{igp}^{ngp} N^{igp}(\xi', \eta')\boldsymbol{T}^{igp}. \tag{6}$$

Therein, the sum over the integration points *igp* with the shape function N^{igp} is evaluated at the "stretched" local coordinates ξ', η' of the adjacent element. ξ, η take values from -1 to 1 in the coordinate system formed by the integration points. This extrapolation using the stretched local coordinates ξ', η' is illustrated in Figure 3.

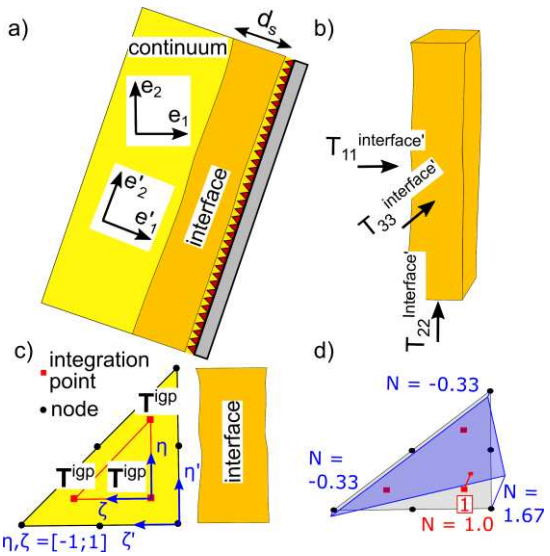

Figure 3. a) Schematic of the global and local coordinate system. b) Mapped stress state in the interface element. c) and d) Extrapolation procedure used to obtain the mapped stress

The stress then has to be rotated into the local coordinate system of the interface element using

$$\boldsymbol{T}^{\text{interface}'} = \boldsymbol{\alpha} \cdot \boldsymbol{T}^{\text{interface}} \cdot \boldsymbol{\alpha}^T. \tag{7}$$

Where $\boldsymbol{\alpha}$ is given by

$$\alpha_{ij} = \boldsymbol{e}'^{(i)} \cdot \boldsymbol{e}^{(j)}. \tag{8}$$

$\boldsymbol{e}^{(j)}$ is the j-th basis vector of the global coordinate system and $\boldsymbol{e}'^{(i)}$ is the i-th basis vector of the local

interface coordinate system. The rotation from global to local coordinate system is displayed in Figure 3.

The shear strain increment $\Delta\boldsymbol{\gamma}$ in the interface can be determined by

$$\tan \Delta\boldsymbol{\gamma} = \frac{\Delta \boldsymbol{g}_T}{d_s}. \tag{9}$$

In Eq. (4), $\Delta \boldsymbol{g}_T$ is the increment of the relative tangential displacement of the surfaces in contact and d_s is the thickness of the shear band. The thickness of the shear band is a function of the median grain diameter of a sand and is approximately $d_s = 5 - 10 \cdot d_{50}$ (see e.g. DeJong et al., 2006). In order to enforce the normal stresses in the interface element to be equivalent to the normal stresses of the adjacent continuum, the interface normal strains required to enforce stress equilibrium are iteratively calculated using

$$\varepsilon_{ij}^{n+1} = \varepsilon_{ij}^{n} - J_{imkl}^{-1} \cdot \left(\mathrm{T}_{kl}^{C'} - \mathrm{T}_{kl}^{\mathrm{interface}'} \right) \delta_{mj}. \tag{10}$$

J_{imkl}^{-1} is the inverse of the constitutive jacobian and $T_{kl}^{C'}$ is the stress due to the consideration of the shear strain increment $\Delta\boldsymbol{\gamma}$. δ_{mj} is the Kronecker symbol. The procedure is repeated n-times until $\left(\mathrm{T}_{kl}^{C'} - \mathrm{T}_{kl}^{\mathrm{interface}'} \right)$ is sufficiently small; hence, stress equilibrium between interface and adjacent continuum is achieved. Note that Eq. (5) only enforces equilibrium of the normal stress components since the shear stress components are in equilibrium automatically. This approach allows for a direct application of continuum models to the modelling of interfaces, potentially incorporating the interface roughness in the constitutive equations. In Staubach et al. (2022b) interface models based on the hypoplastic model with intergranular strain and Sanisand-04 have been formulated. The latter one is used in the simulations presented in the next section.

4 SIMULATOIN OF CENTRIFUGE TESTS

4.1 Description of the tests

Shaking table centrifuge tests of a foundation on liquefiable soil performed by Zeybek and Madabhushi (2017) are back-calculated using the novel numerical schemes. A schematic sketch of the centrifuge test in prototype scale is supplied in Figure 4 (top). A centrifugal acceleration of 70 g has been applied. The numerical analyses have been performed in the model scale and include the spin-up of the centrifuge (up to 70 g). On top of initially medium dense Houston HN31 sand (relative density of 40 %), a brass foundation was placed, which loaded the soil by approximately 135 kPa. The sand was saturated using a fluid with a dynamic viscosity 70-times higher than that of water. A degree of saturation of 99 % was reported for the considered tests (Zeybek and Madabhushi, 2017), which results in a bulk modulus of the pore fluid of approximately 14 MPa. The applied acceleration signal is shown in Figure 4 (bottom) and was applied parallel to the long side of the soil. In model scale, the predominant frequency of the signal is 50 Hz. The permeability of Houston HN31 sand is approximately $1 \cdot 10^{-10}$ m/s (Haigh et al., 2012), which results in a hydraulic conductivity of $1 \cdot 10^{-3}$ m/s. Hence, an influence of the relative acceleration between the solid phase and the pore fluid cannot be ruled out a priori in the present case.

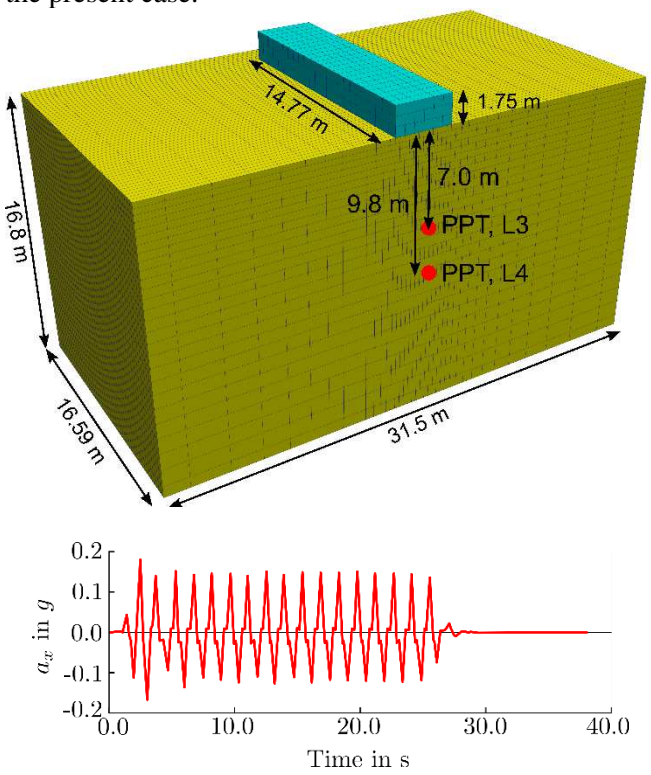

Figure 4. Top: Finite element model and mesh (for the u-U elements) used for the calculation. The location of the pore-pressure transducer (PPT) is given. Bottom: Acceleration-time history of the signal used in the centrifuge test. All quantities are given in prototype scale.

The Sanisand-04 constitutive model (Dafalias & Manzari, 2004) has been used for the numerical analysis. The material constants for the Houston HN31 sand have been determined based on the simulation of undrained monotonic and undrained cyclic triaxial tests reported in Bouferra et al (2017) performed on Hostun-RF sand. Hostun HN31 sand is a successor and behaves mechanically similar to the Hostun-RF sand (Alikarami et al., 2017). The final set of parameters is given in Table 1. The contact between the foundation and the soil was discretized using the Mortar method introduced in Section 3.1. The penalty method was used to enforce the contact constraints for both the solid and the fluid phase. The u-U elements offer an important advantage over the u-p elements in this regard, because drainage at the top surface is automatically only possible for soil not being

in contact with the foundation. Since the foundation moves significantly in lateral direction during the shaking, which can not be known a priori, this is an important aspect, which could only be taken into account by the u-p elements defining a moving boundary condition.

Table 1. Material parameters for the Sanisand-04 model for Hostun-RF/Houston HN31 sand

Parameter	value	Parameter	value
G_0 / kPa	20.0	h_0 / -	10.5
υ / -	0.05	c_h / -	0.55
M_c / -	1.375	n_b / -	1.0
M_e / -	0.942	A_0 / -	0.9
λ_c / -	0.122	n_d / -	1.9
e_0 / -	1.103	z_{max} / -	10.0
ξ / -	0.205	c_z / -	1000
m / -	0.05	p_{atm} / kPa	100

Friction was considered using either a simple Coulomb model with a friction coefficient of $\tan\left(\frac{2}{3}\varphi\right)$ with $\varphi = 32°$ or the Sanisand-04 interface model. For the Coulomb model, a tangential stiffness has to be defined, which was found to influence the results of the simulations strongly since the foundation moves significantly in lateral direction during the shaking. This tangential stiffness can be obtained from interface shear tests and can be correlated with the shear stiffness G^s of the solid. In numgeo, the tangential stiffness is defined based on the stiffness of the adjacent element. The latter option is attractive for the analysis of soils, for which G^s is a function of stress, density and additional state variables. Using the stiffness-based approach, all the effects considered by the adopted continuum model (incrementally non-linearity, effects resulting from load reversals) are reflected in the interface stiffness as well. To do so, at each contact integration point, the constitutive Jacobian $\boldsymbol{J}$ of the adjacent element is determined by calling the material routine. Then, the interface shear stiffness G^c is defined by:

$$G^c = \frac{2\cdot\lambda}{d_s\cdot(ndim\cdot 2-3)}\sum_{i=4}^{2\cdot ndim} J_{ii} \qquad (11)$$

λ is a scaling factor, which has a default value of 1. d_s is the virtual thickness of the shear zone as introduced in Section 3.2 and has the unit of a length. It is set to 5 mm, which is approximately 10-times the median grain of Hostun HN31. $\boldsymbol{J}$ has the unit of stress and G^c is force per volume. Multiplying G^c by the relative tangential displacement increment then gives the shear stress increment.

4.2 Results of the simulations

The top plot in Figure 5 compares the trend of the measured vertical displacement of the centre of the foundation with the predictions by the simulations using u-p and u-U elements, respectively. Both element formulations predict the response well, while an increasing deviation between the formulations can be observed with ongoing seismic loading.

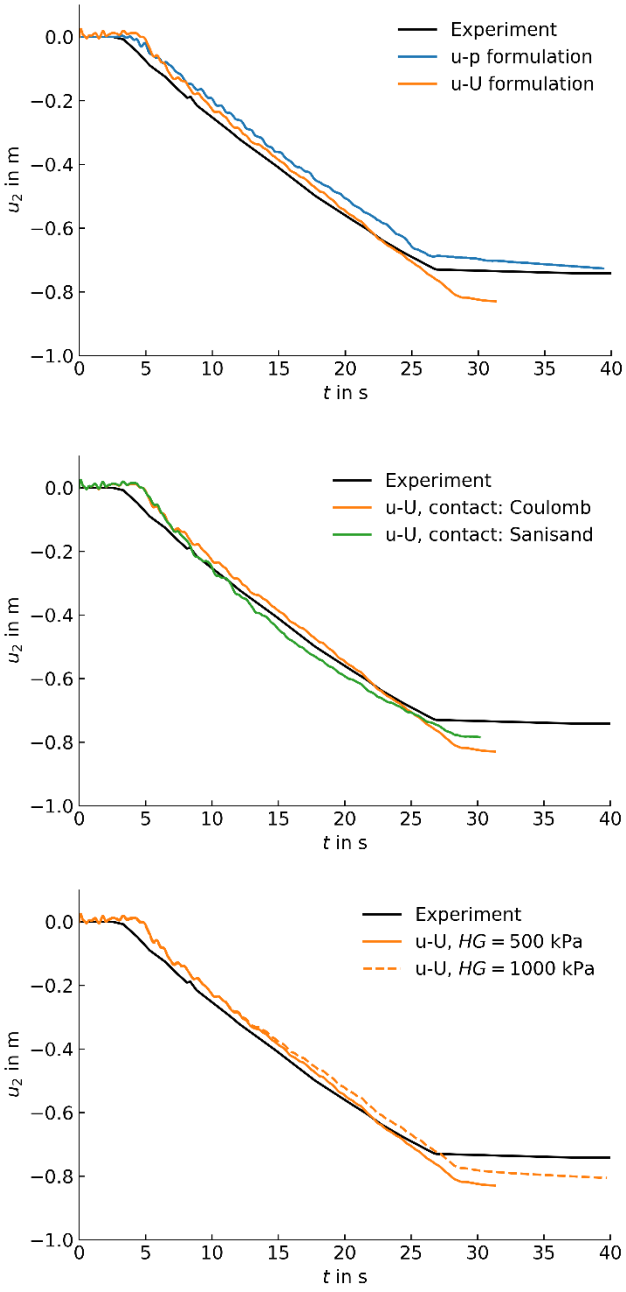

Figure 5. Vertical displacement of the centre of the foundation for the experiment (black) and simulations (coloured). Influence of element formulation (top), interface model (middle) hourglass stiffness for the water phase (bottom)

The two different friction models are compared in the middle of Figure 5. Using the Sanisand interface model, a better accordance in terms of final displacament can be observed, even though a lightly non-linear time history is predicted, which is not in accordance with the measurements. The influence of the value of hourglass stiffness for the water phase introduced in Section 0 is

investigated in Figure 5. A rather limited influence is found, which, however, increases with ongoing time.

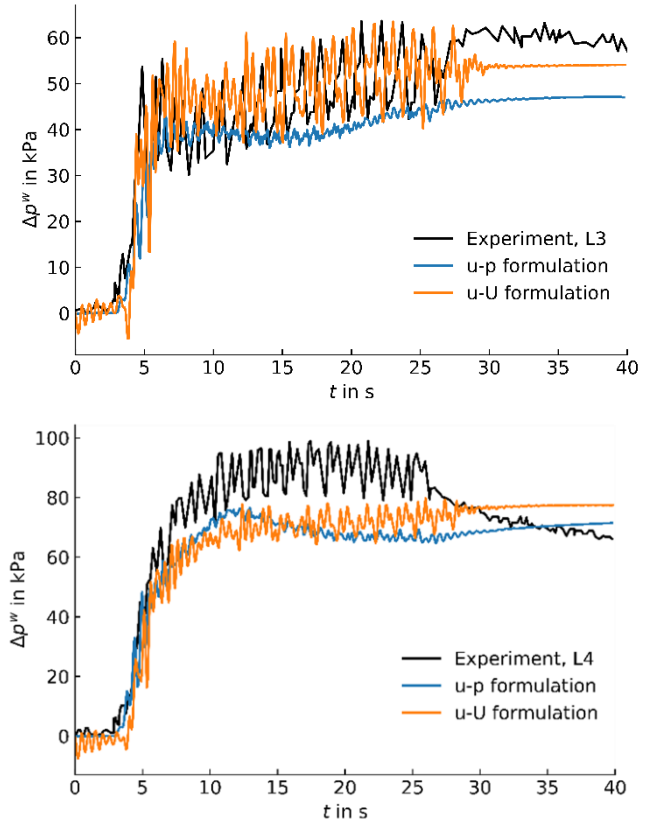

Figure 6. Excess pore water pressure in different depths below the foundation for the values measured in the experiment and simulations using u-p and u-U elements

Finally, the development of excess pore water pressure measured in two different depths below the foundation is compared to simulations using u-p and u-U elements in Figure 6. The u-U elements tend to predict higher amplitudes after 5 s of excitation, which is in better agreement with the measurements compared to the results obtained using u-p elements. Using the reduced integrated u-U elements ($4 \cdot 10^5$ degrees of freedom (dofs) in total and 1 integration point per element), the calculation time was reduced by a factor of 10 compared to the u-p formulation with about $5 \cdot 10^5$ dofs but 27 integration points per element, proving the computational benefit of the u-U elements over the u-p elements.

5 CONCLUSIONS

A one-point integrated, hourglass-enhanced u-U element was introduced, which is found to be numerically more efficient compared to elements based on the u-p element formulation. In addition, special contact constraints for the fluid displacement in contact analyses were implemented and a Sanisand-04 friction model was introduced. The performance of the different numerical schemes was evaluated for the analysis of shaking table tests in a centrifuge. Both the development of settlements and pore fluid pressure were well captured by the simulations.

6 REFERENCES

Alikarami, R., Andò, E., Gkiousas-Kapnisis, M., Torabi, A. and Viggiani, G., 2015. Strain localisation and grain breakage in sand under shearing at high mean stress: insights from in situ X-ray tomography, *Acta Geotechnica*, vol. 10, no. 1,15–30.

Boffi, D., Brezzi, F. and Fortin, M., 2013. *Mixed Finite Element Methods and Applications*, vol. 44. Berlin, Heidelberg: Springer Berlin Heidelberg.

Bouferra, R., Benseddiq, N. and Shahrour, I., 2007. Saturation and Preloading Effects on the Cyclic Behavior of Sand, *International Journal of Geomechanics*, vol. 7, no. 5, 396–401.

Dafalias, Y. F. and Manzari, M. T., 2004. Simple plasticity sand model accounting for fabric change effects, *Journal of Engineering mechanics*, vol. 130, no. 6, 622–634.

Flanagan, D. P. and Belytschko, T., 1989. A uniform strain hexahedron and quadrilateral with orthogonal hourglass control, *International Journal for Numerical Methods in Engineering*, vol. 17, no. 5, 679–706.

Haigh, S. K., Eadington, J. and Madabhushi, S. P. G., 2012. Permeability and stiffness of sands at very low effective stresses, *Géotechnique*, vol. 62, no. 1, 69–75.

Machaček, J., Staubach, P., Tafili, M., Zachert, H., Wichtmann, T. 2021. Investigation of three sophisticated constitutive soil models: From numerical formulations to element tests and the analysis of vibratory pile driving tests, *Computers and Geotechnics*, 138:104276.

Staubach, P., Machaček, J. 2019. Influence of relative acceleration in saturated sand: Analytical approach and simulation of vibratory pile driving tests. *Computers and Geotechnics*, vol. 112, 173–184.

Staubach, P., Machaček, J., Wichtmann, T. 2022a. Mortar contact discretisation methods incorporating interface models based on Hypoplasticity and Sanisand: application to vibratory pile driving. *Computers and Geotechnics*, 146:104677.

Staubach, P., Machaček, J., Wichtmann, T. 2022b. Novel approach to apply existing constitutive soil models to the modelling of interfaces. *International Journal for Numerical and Analytical Methods in Geomechanics*, vol. 46, no. 7, 1241–1271.

Staubach, P., Machaček, J., Tschirschky, L., Wichtmann, T. 2022c. Enhancement of a high-cycle accumulation model by an adaptive strain amplitude and its application to monopile foundations, *International Journal for Numerical and Analytical Methods in Geomechanics*, vol. 46, no. 2, 315–338.

Stutz H., Masin D., Wuttke F. 2016. Enhancement of a hypoplastic model for granular soil–structure interface behavior. *Acta Geotechnica*, vol. 11, no. 6, 1249–1261.

Zeybek, A., Madabhushi, S. 2017. Centrifuge testing to evaluate the liquefaction response of air-injected partially saturated soils beneath shallow foundations. *Bulletin of Earthquake Engineering*, vol. 15, no. 1, 339‑356.